A Letters Journal Exploring the Frontiers of Physics

December 2019

EPL, **128** (2019) 66001 www.epljournal.org
doi: 10.1209/0295-5075/128/66001

Slaved coarsening in ferronematics

Aditya Vats[1], Varsha Banerjee[1] and Sanjay Puri[2]

[1] *Department of Physics, Indian Institute of Technology Delhi - New Delhi 110016, India*
[2] *School of Physical Sciences, Jawaharlal Nehru University - New Delhi 110067, India*

received 25 October 2019; accepted in final form 2 January 2020
published online 31 January 2020

PACS 64.75.Gh – Phase separation and segregation in model systems (hard spheres, Lennard-Jones, etc.)
PACS 77.80.Dj – Domain structure; hysteresis
PACS 68.35.Rh – Phase transitions and critical phenomena

Abstract – We focus on understanding the influence of the two-component coupling in *ferronematics*, a colloidal suspension of magnetic nanoparticles in nematic liquid crystals. Using coarse-grained Landau-de Gennes free energies, we study the ordering dynamics of this complex fluid in $d = 2$ and present a range of analytical and numerical results. Our main observations are: i) slaved coarsening for quench temperatures T intermediate to the critical temperatures of the uncoupled components, ii) slower growth similar to the Lifshitz-Slyozov law ($L \sim t^{1/3}$) for symmetric magneto-nematic coupling, iii) sub-domain morphologies dominated by interfacial defects for asymmetric coupling strengths. These novel results will serve to guide future experiments on this technologically important system.

Liquid crystals (LCs) are a state of matter that is intermediate between conventional solids and liquids with a unique combination of order and fluidity [1–4]. Nematic liquid crystals (NLCs) are the simplest type, and have a natural tendency to align parallel to one another. This preferred direction introduces a strong anisotropy and is described by the nematic director **n**. The NLCs exhibit unique dielectric and diamagnetic properties which are important in versatile applications. The possibility of controlling their optical response by fast reorientation of **n** in a few milliseconds on the application of small electric fields (1–2 mV) is the basis of their utility in modern LC displays and optical imaging [5]. However, due to low values of magnetic susceptibility $\sim 10^{-6}$ (SI units), large magnetic fields $\sim$300 mT are required to actuate them [6]. As a result, most LC devices are mainly driven by electric fields, limiting their applicability in magnetic devices.

The natural question next is whether the introduction of a small quantity of magnetic material can enhance their sensitivity, thereby introducing the possibility of magneto-optic response in addition to the conventional electro-optic response. This idea was first introduced in 1970 by Brochard and de Gennes in their pioneering work [7], which suggested that the nematic molecules could impose ferromagnetic order in the functionalized magnetic nanoparticles (MNPs) due to surface anchoring even in the absence of an external magnetic field! Although intense experimental efforts were made to create stable ferromagnetic suspensions, it was only in 2013 that Mertelj *et al.* obtained the first such suspension of barium hexaferrite magnetic nanoplatelets in pentylcyano-biphenyl LCs with homeotropic anchoring [8]. The stability of the suspension is a consequence of the fine balance between repulsion of defects created by the director field around the MNPs, and the attractive dipole-dipole interaction between their magnetic moments [8–10]. Ever since, this fascinating class of materials called *ferronematics* (FNs) is enjoying increasing interest from academia and industry as well [9,11–20]. There have been proposals to utilize the magneto-mechanical and magneto-optic effects for applications in photonics [18], optical switches [12], complex fluids [13,14], and even particle physics and cosmology [16].

The primary quest after the creation of stable FNs has been to understand the consequences of coupling between the nematic and magnetic components on their equilibrium and non-equilibrium properties. There have been some intriguing experimental observations in this direction. For instance, Shuai *et al.* could use the magneto-nematic coupling to spontaneously create flux closure loops which were sensitive to even the Earth's magnetic field [9]. In another contribution, Mertelj and Lisjak cooled a ferronematic drop from an isotropic phase to the nematic phase and observed domain growth in the presence of a field applied along **n** [10]. Using magneto-optic techniques,

they detected several *bubbles* or *small domain morphologies* with magnetization parallel or anti-parallel to the field which coarsened with time. The domain growth was always accompanied by the flow of the suspension and motion of the defect lines. Mertelj and Lisjak thus demonstrated that the mechanism of domain growth was mediated via a magneto-nematic interaction [14].

The problem of coarsening (or domain growth) after a quench from a disordered phase ($T > T_c$) to an ordered phase ($T < T_c$) holds a special appeal in non-equilibrium physics [21,22]. If the morphology of the coarsening domains is unchanged in time, the system exhibits dynamical scaling and is characterized by a unique divergent length scale $L(t)$. The growth law reveals important details of the free-energy landscape and the relaxation (response) time-scales in the system. In pure and isotropic systems, $L(t) \sim t^{1/z}$, where the growth exponent $1/z$ depends on various factors such as conservation laws, defects and flow fields. For example, systems with non-conserved kinetics obey the Lifshitz-Allen-Cahn (LAC) law: $L(t) \sim t^{1/2}$ which is characteristic of systems with no energy barriers to coarsening [23]. Systems with disorder and competing interactions have a complicated free-energy landscape and a plethora of relaxation time-scales. Domain growth in these systems exhibits a logarithmic behavior in the asymptotic limit [24,25]. What insights can a coarsening experiment provide for FNs, which are described by *two* coupled order parameters? What is the influence of coupling strengths on growth laws? What happens if only one of the two components is in an ordered phase? Motivated by these questions, we develop a time-dependent Ginzburg-Landau (TDGL) formulation for the coupled system to study non-equilibrium properties of FNs rendered unstable after a thermal quench [21,22]. In this letter, we focus on understanding the influence of the magneto-nematic coupling in two-dimensional ($d = 2$) FNs. Such geometries have been realised experimentally in the context of pure NLCs in shallow wells by ensuring that the top and bottom surfaces enforce planar boundary conditions. Consequently, the nematic molecules are primarily confined in a plane and the variations along the height of the sample are negligible. We present a range of analytical and numerical results in our benchmarking study on $d = 2$ FNs, which will serve to guide future experiments on this technologically important system. It will also provide a basis to understand the more complicated defect structures in $d = 3$ FNs and their role in domain growth.

We report three novel results which are as follows: i) for *shallow* quenches ($T_c^N < T < T_c^M$, where N and M refer to nematic and magnetic), the ordering magnetic component *enslaves* the nematic component to coarsen. Their domains are co-aligned. Similar statements hold for quenches such that $T_c^M < T < T_c^N$. ii) Depending on the nature of coupling, domain growth can obey the Lifshitz-Allen-Cahn law $L(t) \sim t^{1/2}$, or a slower $L(t) \sim t^{1/3}$ growth usually referred to as the Lifshitz-Slyozov law. The latter is surprising as it usually characterizes conserved kinetics [21,22], whereas both order parameters here are non-conserved. iii) The structure factor $S(k)$ for the domain morphologies exhibits Porod decay, $S(k) \sim k^{-(d+1)}$, which is characteristic of scattering from sharp interfaces. This contradicts our naive expectation of the generalized Porod tail $S(k) \sim k^{-(d+2)}$ for scattering from vortex defects in continuous-spin models [26].

We use the Landau-de Gennes (LdG) free energy description for the FN [27]. The Landau theory offers a useful phenomenological route to obtain free energy functionals based on the symmetries of the order parameter describing the system. It relies on the fact that, near a phase transition, the free energy of a system can be modeled by the first few terms of a Taylor expansion in the order parameter [28,29]. In the case of FNs, the LdG free energy is a functional of two order parameters: i) the $\mathbf{Q}$-tensor, which contains information about the orientational order of the LC; and ii) the magnetization vector $\mathbf{M}$, which is the magnetic moment of the suspended nanoparticles. We allow $\mathbf{M}$ to have a variable magnitude, including $\mathbf{M} = 0$ to capture segregation effects. In $d = 2$, the $\mathbf{Q}$-tensor is a 2×2 matrix with elements $Q_{ij} = S(\hat{n}_i\hat{n}_j - \delta_{ij}/2)$. The scalar order parameter S measures the fluctuations about the leading eigenvector $\mathbf{n}$ [30]. Further, $\mathrm{Tr}\mathbf{Q} = 0$, $\mathrm{Tr}\mathbf{Q}^2 = 2(Q_{11}^2 + Q_{12}^2) = S^2/2$ and $\mathrm{Tr}\mathbf{Q}^3 = 0$. The free energy for the ferronematic system has been modeled as [1,31]

$$\begin{aligned} G([\mathbf{Q},\mathbf{M}]) = \int \mathrm{d}\mathbf{r}\Bigg[& \frac{\mathbf{A}}{\mathbf{2}}\mathrm{Tr}(\boldsymbol{Q}^2) + \frac{\mathbf{B}}{\mathbf{4}}\mathrm{Tr}(\boldsymbol{Q}^4) + \frac{\mathbf{L}}{\mathbf{2}}|\nabla\mathbf{Q}|^2 \\ & + \frac{\alpha}{2}|\boldsymbol{M}|^2 + \frac{\beta}{4}|\boldsymbol{M}|^4 + \frac{\kappa}{2}|\nabla\boldsymbol{M}|^2 \\ & - \frac{\gamma\mu_0}{2}\sum_{i,j=1}^{2} Q_{ij}M_iM_j\Bigg]. \end{aligned} \tag{1}$$

The first three terms represent the LdG free energy for the nematic component, the next three correspond to the Ginzburg-Landau free energy for the magnetic component and the last term represents the magneto-nematic coupling. To leading order, the coupling term is taken to be the dyadic product of the $\mathbf{Q}$-tensor and $\mathbf{M}$ to respect the rotational invariance of the free energy. The Landau coefficients $A = A_0(T - T_c^N)$ and $\alpha = \alpha_0(T - T_c^M)$, where A_0 and α_0 are positive constants. The parameters B and β are temperature-independent positive material-dependent constants, L and κ are the elastic constants, and γ and μ_0 are the coupling strength and the magnetic permeability respectively. These phenomenological parameters, as will be discussed later, can be estimated from experimentally measured quantities.

Two methods are usually employed to obtain stable FNs [7,8,10]. In the first method, the MNP-NLC mixture is quenched from the (disordered) isotropic phase to the (ordered) nematic phase in the presence of an external magnetic field. This protocol results in a ferronematic

domain with *aligned* magnetic moments [8]. Naturally, such a suspension exhibits maximal magnetization and has been referred to as a *ferromagnetic nematic liquid crystal* by Mertelj *et al.* In the second method, the MNP-NLC suspension is quenched in the absence of an external magnetic field due to which the magnetic moments are parallel to $\mathbf{n}$. They are equally likely to point along $\mathbf{n}$ or $-\mathbf{n}$ directions, leading to vanishing macroscopic magnetization [7,32,33]. For FNs obtained via the first protocol, the free energy has an additional term to represent the coupling between the applied field and the order parameter $\boldsymbol{M}$. Our primary interest is to understand the effects of the magneto-nematic coupling. Therefore, we have not included such a term in eq. (1) to prevent a directional bias in the non-equilibrium studies undertaken. Our study is relevant to FNs obtained via the second method.

The dissipative dynamics of the ferronematic is studied using the coupled time-dependent Ginzburg-Landau (TDGL) equations: $\partial\psi/\partial t = -\Gamma_\psi \delta G[\mathbf{Q},\mathbf{M}]/\delta\psi$, where ψ denotes $\mathbf{Q}$ or $\mathbf{M}$. The terms on the right are the functional derivatives of the free energy functional $G[\mathbf{Q},\mathbf{M}] = \int \mathrm{d}\mathbf{r}\ g(\mathbf{Q},\mathbf{M})$ [22]. A dimensionless form of the TDGL equations can be obtained by introducing rescaled variables $\mathbf{Q} = c_N\mathbf{Q}'$, $\mathbf{M} = c_M\mathbf{M}'$, $\mathbf{r} = c_r\mathbf{r}'$, $t = c_t t'$. Dropping the primes yields the following equations:

$$\frac{1}{\Gamma}\frac{\partial Q_{11}}{\partial t} = \pm Q_{11} - (Q_{11}^2 + Q_{12}^2)Q_{11} + l\nabla^2 Q_{11} + c_1[M_1^2 - M_2^2], \quad (2)$$

$$\frac{1}{\Gamma}\frac{\partial Q_{12}}{\partial t} = \pm Q_{12} - (Q_{11}^2 + Q_{12}^2)Q_{12} + l\nabla^2 Q_{12} + 2c_1[M_1 M_2], \quad (3)$$

$$\frac{\partial M_1}{\partial t} = \pm M_1 - |\mathbf{M}|^2 M_1 + \nabla^2 M_1 + c_2[Q_{11}M_1 + Q_{12}M_2], \quad (4)$$

$$\frac{\partial M_2}{\partial t} = \pm M_2 - |\mathbf{M}|^2 M_2 + \nabla^2 M_2 + c_2[Q_{12}M_1 - Q_{11}M_2]. \quad (5)$$

The dimensionless parameters in eqs. (2)–(5) are

$$c_1 = \frac{\gamma\mu_0|\alpha|}{4|A|\beta}\sqrt{\frac{2B}{|A|}}, \quad c_2 = \frac{\gamma\mu_0}{|\alpha|}\sqrt{\frac{|A|}{2B}}, \qquad l = \frac{|\alpha|L}{2|A|\kappa}, \quad \Gamma = \frac{2|A|\Gamma_Q}{|\alpha|\Gamma_M}. \quad (6)$$

The $\pm$ sign with the first terms on the right depends on whether the corresponding component is above ($-$) or below ($+$) its critical temperature. The parameters c_1 and c_2 are rescaled coupling constants, l sets the scale for relative diffusion of the nematic and magnetic components, and Γ is the relative damping coefficient. For simplicity, we set $l = 1$ and $\Gamma = 1$. Therefore, the only parameters in our model are c_1 and c_2. We emphasize that these originate from the same coupling term in eq. (1). However, in our dimensionless rescaling, they are combined with factors which determine the dimensional scales of the order parameters $\mathbf{Q}$ and $\mathbf{M}$ (see eq. (6)).

Table 1: Coarsening studies which we have undertaken.

Quench temperature	Coupling limits
1) $T_c^N < T < T_c^M$	i) $c_1 \neq 0$, $c_2 = 0$
2) $T_c^M < T < T_c^N$	ii) $c_1 = 0$, $c_2 \neq 0$
3) $T < \min\{T_c^N, T_c^M\}$	iii) $c_1 = c_2 = c$

There are three interesting cases in this problem: 1) $T_c^M > T > T_c^N$, 2) $T_c^N > T > T_c^M$, and 3) $T < \min\{T_c^N, T_c^M\}$. We study these for the following subcases below: (i) $c_1 \neq 0$, $c_2 = 0$, (ii) $c_1 = 0$, $c_2 \neq 0$, and (iii) $c_1 = c_2 = c$, as specified in table 1. A few remarks about the limiting cases are in order. Asymmetric coupling is not unusual, as the order parameters can have vastly different magnitudes in experiment, *e.g.*, large magnetic particle in a bath of small LC molecules. We do not expect to precisely realize c_1 or $c_2 = 0$, or $c_1 = c_2 = c$ in experiments. But due to their tractability, the limiting cases (i)–(iii) provide useful guidelines for experimental studies. We have numerically solved eqs. (2)–(5) by implementing an isotropic Euler discretization on an N^2 lattice ($N = 1024$) with periodic boundary conditions in both directions [34]. The latter are routinely used in simulations to remove edge effects and mimic bulk systems. In any case, all our simulations are in the regime where the length scale of the emergent pattern is much smaller than the simulation box. The discretization mesh sizes were $\Delta t = 0.01$ and $\Delta x = 1.0$. The statistical results do not depend on the time step and mesh size chosen as long as the stability condition is met.

The initial configurations of the nematic and magnetic order parameters were chosen to have small random magnitudes and random orientations. All statistical data were averaged over 100 initial conditions. For $N = 1024$, we do not observe any finite-size effects in our data up to four decades. This was confirmed by carrying out a few test runs with $N = 2048$; the corresponding results did not show any corrections to the $N = 1024$ data. In all figures, the error bars in the data are smaller than the symbol sizes used to depict them. We present here results for some prototypical cases of table 1, and will provide a detailed analysis for all the cases in a longer paper.

Although our primary interest is in coarsening, we first determine the stationary solutions $(\mathbf{Q}^*, \mathbf{M}^*)$ by setting the time and space derivatives to zero in eqs. (2)–(5). We then perform a linear stability analysis by studying the growth of initially small fluctuations $\mathbf{Q}^*(\mathbf{r},0) = \mathbf{Q}^* + \delta\mathbf{Q}^*(\mathbf{r},0)$; $\mathbf{M}^*(\mathbf{r},0) = \mathbf{M}^* + \delta\mathbf{M}^*(\mathbf{r},0)$. In table 2, we present the stable solutions for case 1 in table 1 for all the sub-cases (i)–(iii). They provide a framework to interpret the non-equilibrium evolution of the FN after a temperature quench. Figure 1 shows the morphologies of the nematic (left) and magnetic (right) components for

Table 2: Coupling limits and stable stationary solutions for case 1 of table 1, corresponding to a quench such that $T_c^N < T < T_c^M$.

Coupling limits	Stable stationary solutions: $(M_1^*, M_2^*, Q_{11}^*, Q_{12}^*)$
(i) $c_1 \neq 0$, $c_2 = 0$	$(1, 0, r_Q, 0)$ $r_Q = c_1(1+\hat{S})^{-1}$ $\hat{S} = S^2/4 = 3^{-1}(-2 + a_1 + {a_1}^{-1})$ $a_1 = 2^{1/3}(a_2 + c_1(54 + 27a_2)^{1/2})^{-1/3}$ $a_2 = 2 + c_1^2$
(ii) $c_1 = 0$, $c_2 \neq 0$	$(1, 0, 0, 0)$
(iii) $c_1 = c_2 = c$	$(r_M, 0, r_Q, 0)$ $r_m = [(1+\hat{S})(1+c^2+\hat{S})^{-1}]^{1/2}$ $r_Q = c(1+\hat{S}+c^2)^{-1}$ $\hat{S} = S^2/4 = (1+c^2)(a_1 - 2/3) + {a_1}^{-1}$ $3a_1 = 2^{1/3}(33c^2 + a_2 + {a_3}^{1/2})^{-1/3}$ $a_3 = 1053c^4 + 54c^2a_2$ $a_2 = 2c^2 + 6c^4 + 2c^6$

case 1(i) of table 1. The snapshots are shown at $t = 10^3$ with $c_1 = 4$. In the nematic picture, blue (black) corresponds to $\mathbf{n}$ in the first (or third) quadrant, while green (light gray) corresponds to $\mathbf{n}$ in the second (or fourth) quadrant. In the magnetisation picture, the colours blue (black), red (dark gray), green (light gray) and yellow (white) denote $\mathbf{M}$ lying in the first, second, third and fourth quadrant respectively. We stress that $\mathbf{M}$ is always parallel to $\mathbf{n}$. The magnetic domains coarsen as expected, but what is unusual is the *slaved coarsening* of the nematic phase, and its co-alignment with $\mathbf{M}$. We also find that the magnitudes of $\mathbf{Q}$ and $\mathbf{M}$ are in accordance with the analytical values for the corresponding stable stationary solution.

To quantify the morphologies and domain growth, we define the characteristic length scale $L(t)$ as the distance over which the correlation function decays to (say) 0.2 times its maximum value. If the ordering system is isotropic and characterized by a single length scale, then the correlation function obeys dynamical scaling: $C(\mathbf{r}, t) = f(r/L)$, where $f(x)$ is a scaling function. An equivalent probe is the structure factor $S(\mathbf{k}, t)$, which is the Fourier transform of $C(\mathbf{r}, t)$, and is usually obtained in small-angle scattering experiments. The corresponding dynamical-scaling form is $S(\mathbf{k}, t) = L^d \tilde{f}(kL)$, where $\tilde{f}(p)$ is the Fourier transform of $f(x)$ [22]. Our two-component system has two length scales L_Q and L_M, characterizing the domain growth of the nematic and magnetic components, respectively. For pure nematic and magnetic systems ($c_1 = c_2 = 0$), it is well established that the components obey the LAC law: $L(t) \sim t^{1/2}$ in $d > 2$ and $L(t) \sim [t/\ln t]^{1/2}$ in $d = 2$.

In fig. 2, we show the growth laws for case 1(i) with $c_1 = 3, 4, 5$ and $c_2 = 0$ (left frame); and case 1(iii) with $c_1 = c_2 = c$ for $c = 3, 4, 5$ (right frame). The solid symbols denote $L_Q(t)$ *vs.* t while the open symbols denote $L_M(t)$ *vs.* t. The linear variation on the log-log scale suggests power laws: $L(t) \sim t^{1/z}$. For an accurate determination of the slopes, we evaluated the *effective* growth exponent $\bar{z} = \partial \ln t / \partial \ln L(t)$. The insets in figs. 2(a), (b) show $\bar{z}$ *vs.* t on a semi-log scale. The dashed lines indicate the exponent values $z = 2$ and 3. The data for case 1(iii) is consistent with the LAC law for both components. Thus the slaved nematic order parameter, which is naturally isotropic, is driven to ordering by the magnetisation field. Both these fields show the same growth law. We emphasise that the exponent $z \gtrsim 2$ because of the logarithmic correction arising in the growth law for $d = 2$.

The data for case 1(iii) in fig. 2(b) is the second unexpected outcome of our study. Both the systems indeed coarsen together, but now the growth law is much closer to $L(t) \sim t^{1/3}$. The latter, usually referred to as the Lifshitz-Slyozov (LS) law, is characteristic of systems with conserved dynamics though both order parameters are non-conserved in the present case! Our study indicates that the LS-like law is observed in all three cases of table 1 for a symmetric coupling $c_1 = c_2 = c$ between components.

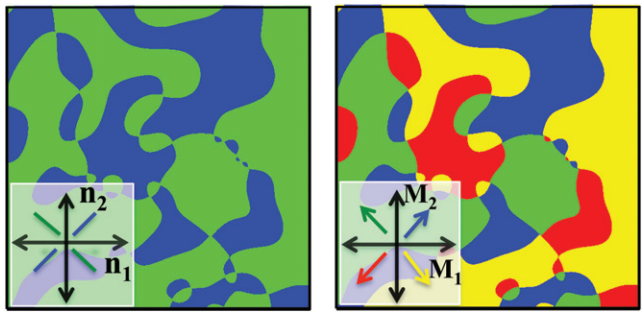

Fig. 1: Morphology snapshots corresponding to case 1(i) of table 1 for the nematic (left) and magnetic (right) components at time $t = 10^3$ with coupling constants $c_1 = 4, c_2 = 0$. The colour code shown in the insets is detailed in the text.

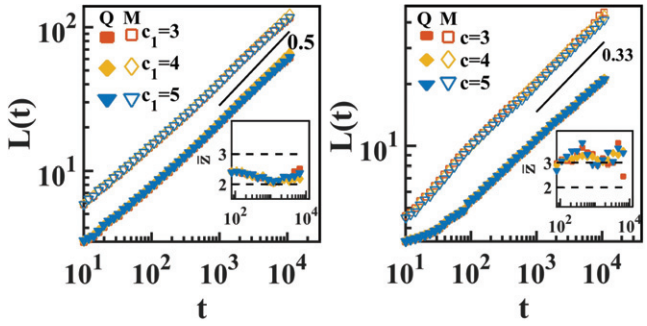

Fig. 2: Growth laws on a log-log scale for case 1(i) (left) and case 1(iii) (right) of table 1. The solid (open) symbols denote the nematic (magnetic) component. The insets show the effective growth exponent $\bar{z} = [\mathrm{d}(\ln L)/\mathrm{d}(\ln t)]^{-1}$ *vs.* t. The dashed lines corresponds to $\bar{z} = 2$ (left) and $\bar{z} = 3$ (right).

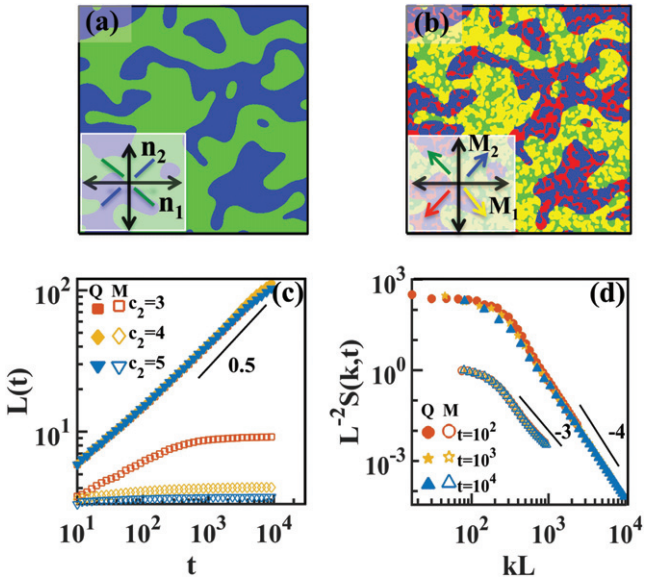

Fig. 3: (a) Nematic and (b) magnetic morphologies for the case 3(ii) of table 1 with $c_1 = 0, c_2 = 4$. Growth laws $L(t)$ *vs.* t for specified values of c_2 are shown in (c). The scaled structure factor data, $L^{-2}S(k,t)$ *vs.* kL, at the specified times t is shown in (d). The solid (open) symbols in (c) and (d) denote the nematic (magnetic) component.

The nature of the defects can be interpreted from the tail of the structure factor [26]. For the cases 1(i) and 1(iii), we find that the nematic and magnetic components exhibit the *generalized Porod decay* $S(k,t) \sim k^{-(d+n)} = k^{-4}$ for $d = 2$, $n = 2$. This is characteristic of scattering from vortex defects in XY-type spin models [26]. As a matter of fact, we observe the k^{-4} decay for all the cases in table 1 when (i) $c_1 \neq 0$, $c_2 = 0$, and (iii) $c_1 = c_2 = c$.

Finally, we present some results for the situation when the nematic field evolves freely but the magnetisation field is driven by the nematic field, *i.e.*, $c_1 = 0$, $c_2 \neq 0$. We focus on case 3(ii) of table 1 with $T < \min\{T_c^N, T_c^M\}$ so that both the components are in the ordered phase. The corresponding results are provided in fig. 3. In (a) and (b) we show the nematic and magnetic morphologies for $c_2 = 4$ and $t = 10^3$. We see that the components are aligned, *i.e.*, $\mathbf{n} \parallel \mathbf{M}$. However, the magnetic component exhibits a small sub-domain morphology (SDM) due to the two possible alignments, $\mathbf{n} \parallel \mathbf{M}$ and $\mathbf{n} \parallel -\mathbf{M}$, with the same energy. The sub-domain gradients in $\mathbf{M}$ have a cost in terms of the surface tension, but this is estimated to be negligible compared to the entropic gain due to the formation of the SDM. The magnitudes of $\mathbf{Q}$ and $\mathbf{M}$ agree with the corresponding stable stationary solutions that we have evaluated for case 3(ii) (not presented here). In fig. 3(c), we depict the growth laws for $c_2 = 3, 4, 5$. While $L_Q(t) \sim t^{1/2}$ as expected, $L_M(t)$ saturates to L_M^S due to the formation of the SDM. The size of the sub-domains or the saturation length scale is set by c_2, and decreases with increasing magneto-nematic coupling. In the uncoupled limit $c_2 \to 0$, we expect $L_M^S \to \infty$. More insights on the SDM are provided by the scaled structure factor, $L^{-2}S(k,t)$ *vs.* kL, plotted in fig. 3(d) for $c_2 = 4$. As expected, $S_Q(k,t)$ exhibits a generalized Porod tail $S_Q \sim k^{-4}$, due to scattering off vortex-like defects in fig. 3(a). However, $S_M(k,t)$ shows the usual Porod tail $S_M \sim k^{-3}$! This is a result of scattering from the sharp "interfaces" between the sub-domains with magnetization $\mathbf{M}$ and $-\mathbf{M}$. Though $\mathbf{M}$ is a continuous order parameter, the nematic coupling enforces a discrete up-down symmetry for $\mathbf{M}$ in the SDM. We find that the SDM and the k^{-3} law exhibited by the magnetic component is generic to $c_1 = 0$, $c_2 \neq 0$, see table 1.

So what are the novel insights from this first coarsening study of a ferronematic? Our TDGL formulation for the FN has allowed us to understand the effects of magneto-nematic coupling on morphologies and growth laws. Rather than the nature of the quench, *e.g.*, shallow (say $T_c^N < T < T_c^M$) or deep ($T < \min\{T_c^N, T_c^M\}$), it is the relative coupling strengths of c_1 and c_2 which dictate the systemic behavior. There are three new observations from our study: i) slaved coarsening for quench temperatures T between the critical temperatures of the uncoupled components, ii) slower growth similar to Lifshitz-Slyozov ($L(t) \sim t^{1/3}$) law for symmetric magneto-nematic coupling ($c_1 = c_2 = c$), iii) sub-domain morphologies dominated by interfacial defects for asymmetric coupling strengths ($c_1 = 0, c_2 \neq 0$).

Finally, what is the experimental relevance of this simplistic model? The Landau coefficients A, B and L are related to experimentally measured quantities like the critical temperature, the latent heat of transition and the order parameter [2]. Similarly, coefficients α, β and κ can be evaluated from the measurements of magnetization and susceptibility [35]. The coupling constant γ has been estimated from the reversal fields of hysteresis loops [8]. In principle therefore, it is possible to determine our dimensional scales and the dimensionless coupling constants c_1 and c_2. However, the existing experimental data on FNs are in the presence of external magnetic fields, which biases the response functions. So it is not possible to obtain estimates of our scaled parameters at this juncture. In the stable FNs created so far, $T_c^N < T_c^M$. Thus, of the three cases we have studied (see table 1), the most relevant are 1 and 3. In this emergent research area of FNs, combined experimental and theoretical efforts are needed to understand the fundamentally rich and technologically important properties. We hope our theoretical results will propose and guide coarsening experiments in FNs. Our work is a step in this direction.

* * *

AV acknowledges UGC, India for a research fellowship. AV and VB gratefully acknowledge partial financial support from DST-UKIERI and the HPC facility of IIT Delhi for the computational resources. SP is grateful

to the Department of Science and Technology (India) for support through a J. C. Bose fellowship.

REFERENCES

[1] Prost J. and de Gennes P. G., *The Physics of Liquid Crystals* (Oxford University Press) 1995.
[2] Priestly E., *Introduction to Liquid Crystals* (Springer) 2012.
[3] Stephen M. J. and Straley J. P., *Rev. Mod. Phys.*, **46** (1974) 617.
[4] Lavrentovich O. and Kleman M., *Cholesteric Liquid Crystals: Defects and Topology* (Springer) 2001.
[5] Chen H. W., Lee J. H., Lin B. Y., Chen S. and Wu S. T., *Light Sci. Appl.*, **7** (2018) 17168.
[6] de Gennes P. G., *Mol. Cryst. Liq. Cryst.*, **7** (1969) 325.
[7] Brochard F. and de Gennes P. G., *J. Phys.*, **31** (691) 1970.
[8] Mertelj A., Lisjak D., Drofenik M. and Čopič M., *Nature*, **504** (2013) 237.
[9] Shuai M., Klittnick A., Shen Y., Smith G. P., Tuchband M. R., Zhu C., Petschek R. G., Mertelj A., Lisjak D., Čopič M. *et al.*, *Nat. Commun.*, **7** (2016) 10394.
[10] Mertelj A. and Lisjak D., *Liq. Cryst. Rev.*, **5** (2017) 1.
[11] Mertelj A., Osterman N., Lisjak D. and Čopič M., *Soft Matter*, **10** (2014) 9065.
[12] Liu Q., Ackerman P. J., Lubensky T. C. and Smalyukh I. I., *Proc. Natl. Acad. Sci.*, **113** (2016) 10479.
[13] Potisk T., Svenšek D., Brand H. R., Pleiner H., Lisjak D., Osterman N., Mertelj A. *et al.*, *Phys. Rev. Lett.*, **119** (2017) 097802.
[14] Potisk T., Mertelj A., Sebastián N., Osterman N., Lisjak D., Brand H. R., Pleiner H. and Svenšek D., *Phys. Rev. E*, **97** (2018) 012701.
[15] Zhang Q., Ackerman P. J., Liu Q., Smalyukh I. I. *et al.*, *Phys. Rev. Lett.*, **115** (2015) 097802.
[16] Tai J. S. B., Ackerman P. J. and Smalyukh I. I., *Proc. Natl. Acad. Sci.*, **115** (2018) 921.
[17] Rupnik P. M., Lisjak D., Čopič M. and Mertelj A., *Liq. Cryst.*, **42** (2015) 1684.
[18] Ackerman P. J. and Smalyukh I. I., *Nat. Mater.*, **16** (2017) 426.
[19] Zarubin G., Bier M. and Dietrich S., *J. Chem. Phys.*, **149** (2018) 054505.
[20] Peroukidis S. D. and Klapp S. H., *Phys. Rev. E*, **92** (2015) 010501.
[21] Bray A. J., *Adv. Phys.*, **51** (2002) 481.
[22] Puri S. and Wadhawan V., *Kinetics of Phase Transitions* (CRC Press, Boca Raton) 2009.
[23] Allen S. M. and Cahn J. W., *Acta Metall.*, **27** (1979) 1085.
[24] Lippiello E., Mukherjee A., Puri S. and Zannetti M., *EPL*, **90** (2010) 46006.
[25] Corberi F., Lippiello E., Mukherjee A., Puri S. and Zannetti M., *Phys. Rev. E*, **85** (2012) 021141.
[26] Bray A. J. and Puri S., *Phys. Rev. Lett.*, **67** (1991) 2670.
[27] Mottram N. J. and Newton C. J. P., arXiv preprint, arXiv:1409.3542 (2014).
[28] Binder K., *Phys. Rev. B*, **8** (1973) 3423.
[29] Hohenberg P. C. and Halperin B. I., *Rev. Mod. Phys.*, **49** (1977) 435.
[30] Luo C., Majumdar A. and Erban R., *Phys. Rev. E*, **85** (2012) 061702.
[31] Pleiner H., Jarkova E., Müller H. W. and Brand H. R., *Magnetohydrodynamics*, **37** (2001) 146.
[32] Petrov D. A. and Zakhlevnykh A. N., *Mol. Cryst. Liq. Cryst.*, **557** (2012) 60.
[33] Zakhlevnykh A. N. and Petrov D., *J. Magn. Magn. Mater.*, **401** (2016) 188.
[34] Kincaid D. and Cheney E. W., *Numerical Analysis: Mathematics of Scientific Computing* (American Mathematical Society) 2009.
[35] Hohenberg P. C. and Krekhov A. P., *Phys. Rep.*, **572** (2015) 1.